Isotopic composition of *Conomurex fasciatus* shells as an environmental proxy for the Red Sea

N. Hausmann [a], *, A.C. Colonese [a], A. de Lima Ponzoni [b], Y. Hancock [b], M. Meredith-Williams [a, c], M.J. Leng [d, e], G.N. Bailey [f]

[a] BioArCh, Department of Archaeology, University of York, Biology S. Block, York YO10 5DD, UK
[b] Department of Physics, University of York, Heslington, York YO10 5DD, UK
[c] Department of Anthropology, University of Auckland, Private Bag 92019, Auckland 1, New Zealand
[d] NERC Isotope Geosciences Facilities, British Geological Survey, Nottingham NG12 5GG, UK
[e] Centre for Environmental Geochemistry, University of Nottingham, Nottingham NG7 2RD, UK
[f] Department of Archaeology, University of York, The King's Manor, York YO1 7EP, UK

ARTICLE INFO

ABSTRACT

The marine gastropod *Conomurex fasciatus* (Born 1778) is the main component of thousands of shell middens on the Farasan Islands in the southern Red Sea. The middens date from 6500 to 4500 cal BP and cover the period of increased aridification over the region. No general research on *C. fasciatus* has been carried out before and basic information about the species is mostly speculative. To test if *C. fasciatus* shells can be used as a recorder of climate variability, we collected living specimens from the Farasan Islands, in Saudi Arabia, over a 1.5 year period. This area receives almost no precipitation and sea surface salinity is extremely high (38–39 psu), and sea surface temperature (SST) ranges from +26.5 °C to +34.9 °C.

Raman spectroscopy results on modern *C. fasciatus* shell samples show these specimens to be aragonitic. Ground fragments from archaeological *C. fasciatus* shells used for isotope analyses were also measured by Raman spectroscopy and shown to be well preserved against diagenetic alterations leading to aragonite to calcite transformation. Measured shell-edge $\delta^{18}O$ values range from −0.5‰ to −1.7‰. Calculated modern shell edge temperatures from these $\delta^{18}O$ values correlate with modern SST measured on site with an error of ±2.4 °C. Two different growth rates occurred in the shells of *C. fasciatus*. The measurement of growth increments in the lip part of adult specimens indicates a tide-related growth rate of ~13 mm/year. Sequential $\delta^{18}O$ data from juvenile parts of the shell indicates a faster growth rate of ~90 mm/year. This growth rate and the correlation of $\delta^{18}O$ with measured temperatures allows the use of *C. fasciatus* shell $\delta^{18}O$ as a palaeoclimate proxy.

© 2015 Elsevier Ltd and INQUA. All rights reserved.

1. Introduction

The Farasan Island shell middens in the southern Red Sea suggest intense coastal shellfish exploitation (Alsharekh and Bailey, 2014; Bailey et al., 2007, 2013). With over 3000 recorded shell middens, they represent some of the densest accumulations of coastal middens in the world (Fig. 1). The middens are exceptional, especially when compared to the small number of prehistoric coastal sites on the Arabian mainland located 40 km farther east (Durrani, 2005).

The Farasan middens accumulated over a period from 6500 to c. 4500 cal BP (Bailey et al., 2013). The changing distribution of sites suggests a rapid change in sea level, in the overall environment, as well as in exploitation intensity (Meredith-Williams et al., 2014a). The time frame of exploitation partially covers climate change from a humid to more arid conditions during the mid-Holocene from around 7000 to 6000 cal BP (Adamson et al., 1980; Arz et al.,2003; Bar-Matthews et al., 1999; van Campo et al., 1982; Fleitmann et al., 2007; Gasse, 2000; Hoelzmann et al., 1998; Pachur and Kröpelin, 1987; Rossignol-Strick, 1983, 1985). Humid conditions are associated with a northward displacement of the summer monsoon due to a shift in the intertropical convergence zone (ITCZ) to 23°N (Biton et al., 2010). After c. 6000 cal BP, it is thought that conditions were more arid, possibly as a result of ITCZ moving southward
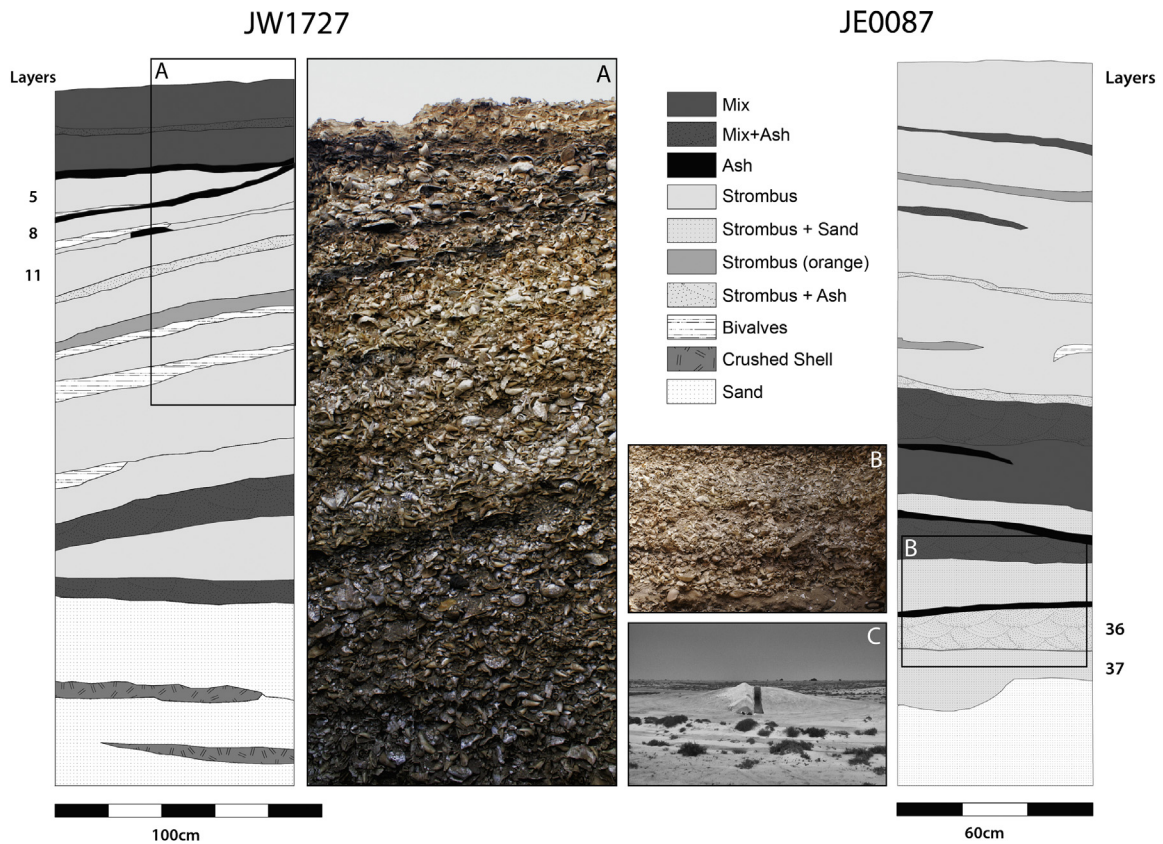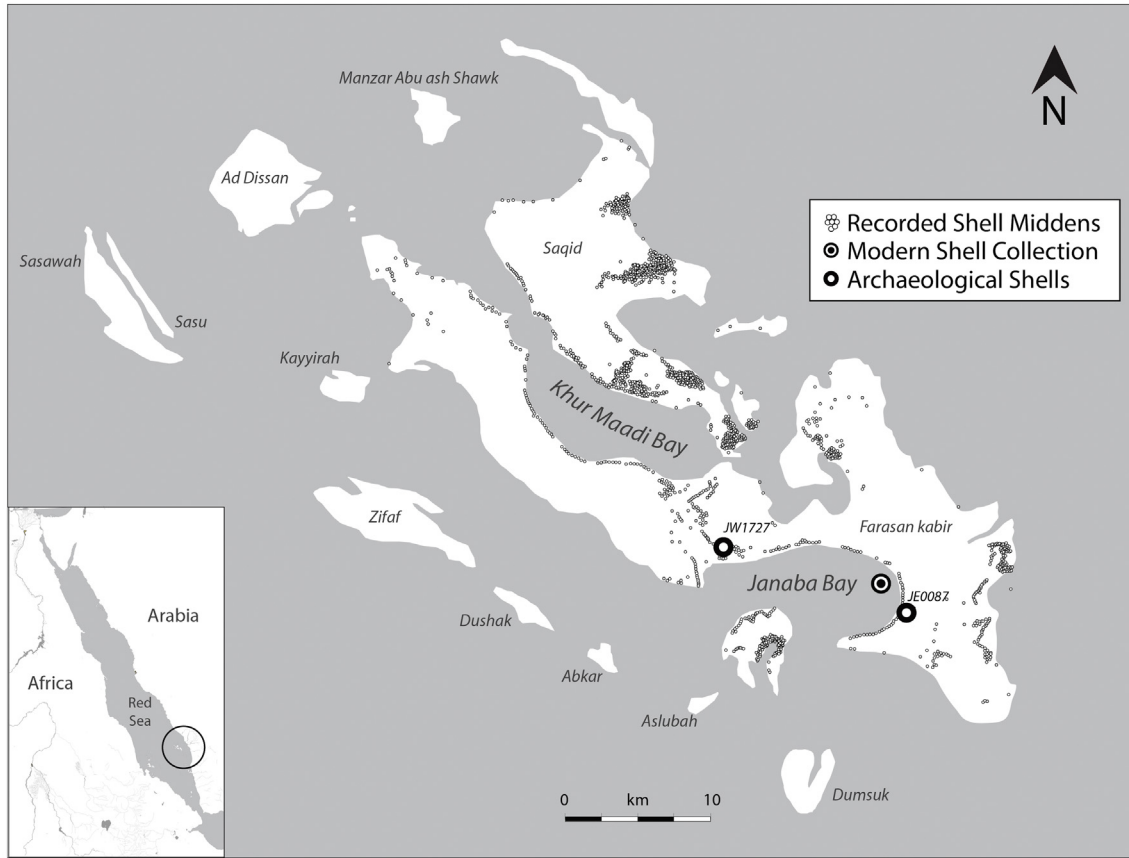
Fig. 1. Study area and overview of shell midden cluster on the Farasan Archipelago, southern Red Sea. Panels A and B show stratigraphic context of archaeological samples. Panel C shows site JE0087 and location of trench.

(Fleitmann et al., 2007). This would have caused an increase in desertification (Bray and Stokes, 2004), indicated by increased dolomite in marine cores from the northern Indian Ocean (Sirocko et al., 1993).

The archaeological record from the Farasan Islands has the potential to supply climate and environmental information, and offers unique insights into environmental limits and opportunities for past societies. In particular the isotope ($\delta^{18}O$ and $\delta^{13}C$) composition of shell carbonate has proven to be a helpful tool in environmental (Arrighetti et al., 2012; Finstad et al., 2013) and archaeological research (Andrus, 2011; Colonese et al., 2009; Leng and Lewis, 2014; Mannino et al., 2003; see also; Thomas, 2015). In marine carbonates, $\delta^{18}O$ values are controlled by the temperature and the $\delta^{18}O$ of the ambient water. Precipitation and freshwater inflow can have a large impact on the $\delta^{18}O$ of the ambient water, as rainwater and water from estuaries has low $\delta^{18}O$, and thus freshwater can impact on the recorded isotopic signal from shelly material (Schweikhardt et al., 2011). Additionally, evaporation processes can enrich the ambient water in ^{18}O.

In shell carbonates, further effects can be significant for the interpretation of stable isotope ratios. Endogenous processes such as age, growth, reproduction, and environmental factors such as food availability and temperature can influence the animal activity and shell isotopic record (Schöne, 2008).

$\delta^{13}C$ from shell carbonates can be complicated because of the multiple sources of carbon. It is generally thought that the dominant control is the $\delta^{13}C$ of dissolved inorganic carbon (DIC) which gets transferred to the shell through fluid exchange (e.g. McConnaughey and Gillikin, 2008). Nevertheless, studies also reveal that (especially) for grazers the contribution of metabolic carbon, which is isotopically light, may be considerable (up to ~40‰, Gillikin et al., 2007), depending on the availability of food sources (e.g. Chauvaud et al., 2011).

Here, we aim to unravel some of the environmental and metabolic factors influencing the stable isotope composition of *C. fasciatus*. We analyse for the first time the $\delta^{13}C$ and $\delta^{18}O$ composition of modern and archaeological shells of *Conomurex fasciatus* (Born, 1778), the most intensively exploited marine gastropod in the Farasan shell middens of the Red Sea (Bailey et al., 2013). We explore the potential of shell $\delta^{13}C$ and $\delta^{18}O$ to provide insights into Holocene environmental conditions and seasonal patterns of coastal exploitation in the region.

2. Background

2.1. Area description

The Farasan archipelago is part of the Arabian continental shelf, the water depth is between 0 and 100 m deep (punctuated by deep depressions caused by salt tectonics) before the shelf drops off into the underwater canyon in the Red Sea. This area is highly influenced by tectonic activity and salt-domes that uplift the submerged fossil reef limestone that largely make up the Farasan Islands (Bantan, 1999). Farasan al-Kabir has suffered the most intense rifting with areas of uplift reaching heights of 70 m above sea level. Palaeoshorelines are present in the guise of former cliffs that have been undercut by wave action. The area has a subtropical desert climate. During the period of observation, the sea surface temperature (SST) ranged from +26.5 °C in January 2013 (winter) to +34.9 °C in September 2013 (summer) (Fig. 2). Precipitation patterns at this site are controlled by the Indian monsoon (Rossignol-Strick, 1985). Rain only falls in short episodes, and it is not enough to sustain permanent wadis or subsurface freshwater flow into the sea. Sea surface salinity (SSS) is among the highest in the world and ranges from 36.9 to 38.8 psu (Fig. 2). In the southern Red Sea it is influenced by evaporation and also by the seasonal inflow from the Indian Ocean through the Bab al Mandab strait (Siddall et al., 2004; Aiki et al., 2006; Trommer et al., 2010; Bouilloux et al., 2013; Raitsos et al., 2013, 2015). Surface water, controlled by the seasonal monsoon wind reversal, is forced into the Red Sea from October to April and out from the Red Sea from May to September. This mechanism transports nutrients and high amounts of phytoplankton from the Gulf of Aden towards the Farasan Islands which substantially influences the marine ecosystem (Bruckner et al., 2011).

2.2. Archaeological background

The number of recorded Farasan shell middens is more than 3000 and not all have been completely surveyed. Radiocarbon dates for the middens so far dated range from 6500 to 4500 cal BP (Bailey et al., 2013). The actual occupation duration of individual middens is still a part of ongoing research as there are many different phases of occupation and clusters of middens that align with different palaeoshorelines.

The shell middens range from small deflated clusters of shells to 6 m high mounds of tightly packed shell material. In the mounds there is little or no fine grained sediment and most layers are clast-supported. Nearly all of the excavated shell middens contain significant amounts of *C. fasciatus* shells (Bailey et al., 2013).

Sites on Farasan are broadly comparable to the shell middens in southwestern Saudi Arabia and northern Yemen, where similar mounds attributed to the Neolithic occur. The lithic assemblages of the mainland shell middens are considerably more abundant and they are mostly linked to the Arabian Bifacial Tradition (Zarins et al., 1981). In southwestern Arabia middens with pottery have previously only been dated to the Bronze Age, as the ceramics show similarities to ceramics found on Bronze Age sites elsewhere in Arabia (Durrani, 2005). Stratified pottery found in the Farasan shell mounds, JW1727 and JE0087, has been radiocarbon-dated to an earlier period (Table 1).

Table 1
Radiocarbon dates from JW1727 and JE0087.

| Site	Lab no.	Layer	^{14}C-age	Mar. Res. Corr.	BP range 2 sigma	Material	Species
JE0087	OxA 28,619	2	5692 ± 30	−100 ± 50	6077–5920	Shell	*C. fasciatus*
	OxA 28,797	10	5698 ± 33	−100 ± 50	6089–5929	Shell	*C. fasciatus*
	OxA 28,386	14	5132 ± 31		5927–5769	Charcoal	Unidentified
	OxA 28,072	14	5718 ± 30	−100 ± 50	6093–5934	Shell	*C. fasciatus*
	OxA 28,413	27	5232 ± 29		5995–5935	Charcoal	Unidentified
	OxA 28,860	27	5673 ± 31	−100 ± 50	6032–5889	Shell	*C. fasciatus*
	OxA 28,618	35	6185 ± 31	−100 ± 50	6580–6431	Shell	*C. fasciatus*
JW1727	OxA 28,009	2	4851 ± 31	−100 ± 50	5108–4873	Shell	(*Brachidontes* sp.)
	OxA 27,890	17	4202 ± 29		4835–4660	Charcoal	Unidentified
	OxA 27,889	23	4287 ± 29		4861–4838	Charcoal	Unidentified
	OxA 28,617	23	4701 ± 28	−100 ± 50	4907–4735	Shell	(*Brachidontes* sp.)
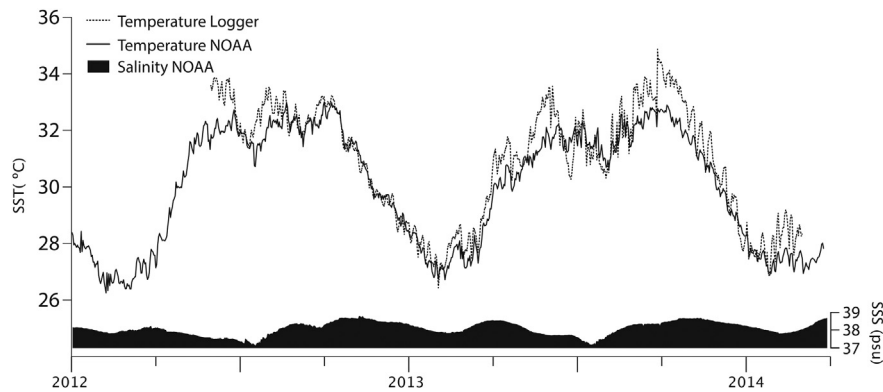
Fig. 2. SST and SSS from January 2012 to March 2014. SST and SSS provided by the National Oceanic and Atmospheric Administration (NOAA): GLOBAL-HYCOM remote sensor, 60 min, available at http://ecoforecast.coral.noaa.gov/index/0/FARS1/station-home for the Farasan Islands (FARS1).

2.3. Conomurex fasciatus ecology and distribution

The marine gastropod *Conomurex fasciatus* (Born 1778) (also *Strombus fasciatus*, the lined conch) is common in the Red Sea. It is herbivorous and well adapted to the warm climate and highly saline environments. Adult specimens are between 25 and 50 mm in length. Their lifespan is unknown but it is assumed that they live for only a few years, a similar duration to the smaller Strombid species (Walls, 1980). It is generally believed that *C. fasciatus* prefers to live in calm water on muddy substrates (Sharabati, 1984). However, our observations in the Farasan Islands indicate that *C. fasciatus* tends to occur in wave impacted shallow waters, on sandy deposits with little vegetation. The

(Alsharekh and Bailey, 2014)) every three months between November 2012 and December 2013 (Table 2; Fig. 1). Although the sampled subtidal zone contained many mollusc species, *C. fasciatus* was relatively scarce and thus only a few specimens were collected for stable isotope analysis per sampling visit (n = 2—5). Surveys around the island and on other islands also yielded very low numbers of *C. fasciatus*. The difference between populations today and during the occupation of the shell middens must have been considerable. Bearing in mind that hundreds of thousands of *C. fasciatus* shells can be contained in a single midden, it is likely that conditions for the gastropod have changed significantly. It is interesting to consider the impact of intense past exploitation on the shellfish population (Bailey et al., 2013).

Table 2
Average differences between SST (reported in °C) estimated from $\delta^{18}O_S$ and SST values by data logger.

Collection date	Average shell edge $\delta^{18}O$		Average shell edge $\delta^{13}C$		Calculated SST	Daily SST	Difference daily SST	Month SST	Difference Monthly SST	Measured water $\delta^{18}O$	Daily SSS (psu)
16.11.12 n = 2	−0.90	±0.42	+1.55	±0.07	30.7 ± 1.8	30.6	−0.2	31.5	0.8	1.71	38.63
18.02.13 n = 3	−0.56	±0.07	+1.24	±0.15	28.0 ± 0.3	27.7	−0.3	27.2	−0.8	1.40	37.87
28.02.13 n = 2	−0.54	±0.05	+0.80	±0.3	27.5 ± 0.2	27.5	0.0	27.4	−0.2	1.32	38.03
30.05.13 n = 2	−1.55	±0.07	+1.25	±0.07	31.5 ± 0.3	32.1	0.6	31.1	−0.4	1.22	37.73
28.09.13 n = 5	−1.47	±0.13	+1.81	±0.23	32.2 ± 0.6	32.8	0.6	32.3	0.1	1.47	38.26
11.12.13 n = 2	−0.67	±0.08	+1.36	±0.01	30.8 ± 0.3	29.7	−1.0	30.5	−0.3	1.94	38.39

overall scarcity of the species around the Farasan Islands in particular made more detailed observations difficult to obtain. *C. fasciatus* is potentially very mobile as the mollusc uses its foot to jump through the water to change locality. During warmer periods, *C. fasciatus* is often found in thick layers of vegetation, possibly for camouflage. This behavior is very similar to that of *S. tricornus*, which is found in similar habitats but is a much larger species (Sharabati, 1984).

Research on the growth rate and $\delta^{18}O$ values of the cross-lamellar structure of *S. gigas* shells in a tropical climate has shown that the shell material can be used as an environmental proxy (Radermacher et al., 2009). Similar conclusions were reached by Cornu et al. (1993) for *S. bubonius*, Wefer and Killingley (1980) for *S. gigas* and *S. costatus*, and Geary et al. (1992) for *S. pugilis*.

3. Material and methods

3.1. Modern shell collections

Living specimens (n = 16) were collected in the subtidal zone of Janaba Bay (where several shell middens have been excavated

After live collection, *C. fasciatus* specimens were prepared for analysis by placing the animals in 5% NaClO. This secured an exact time of death. Samples remained in the solution for 48 h. Afterwards they were rinsed, and their body tissue was removed. Samples were transported to the laboratory in York (BioArCh), rinsed and sonicated with ultra-pure water, and oven-dried at 40 °C.

Simultaneously, water samples for $\delta^{18}O$ analysis (n = 6) were collected at Janaba Bay as a reference for the $\delta^{18}O$ composition of the ambient water of the shells and to account for seasonal changes in salinity that could impact on the $\delta^{18}O$ composition in the shell apart from the seasonal change in temperature. Additionally, we collected water samples in a more enclosed area (Khur Maadi Bay) between the two main islands Farasan Kabir and Saqid (n = 3). Different from the coast in Janaba Bay, which experiences heavy wave action and constantly exchanges water with the open sea (Fig. 1), the sampling location in Khur Maadi Bay is in shallow calm waters (<10 m). Due to its sheltered location it experiences less mixing with the Red Sea water outside the archipelago. These samples were used to compare the seasonal effects of evaporation on the $\delta^{18}O$ composition

between exposed (Janaba Bay) and enclosed (Khur Maadi Bay) mollusc habitats. However, the absence of modern *C. fasciatus* in Khur Maadi bay prevented comparison of the $\delta^{18}O$ composition of shell carbonate.

Daily SSTs were measured in 1.5 m depth close to the shell collection site at Janaba Bay from May 2012 to February 2014 (Star Oddi DST CTD, data logger). SST and SSS values were also provided by the National Oceanic and Atmospheric Administration (NOAA). The data were measured hourly by a GLOBAL-HYCOM remote sensor (available for the Farasan Islands (FARS1 at http://ecoforecast.coral.noaa.gov/index/0/FARS1/station-home).

3.2. Archaeological shells

Two sets of archaeological shells were chosen for stable isotope analysis (n = 6). The samples belong to two shell middens (JE0087 and JW1727) dated to 6000–6500 and 4800 cal BP, respectively (Fig. 1, Table 1.). The samples were extracted in 2013 by excavating a trench from the edge to the centre of the mound and taking two column samples out of the section to provide a stratigraphic record of shell composition throughout the midden.

Shell midden JW1727 is located in the northwest part of Janaba Bay which is now 0.75 km from the sea due to local sea level change. It is about 2 m in height and 30 m across, and located on a sand ridge along a palaeo-coastline and in line with several dozens of similar shell middens.

Apart from several broken potsherds, no other artefacts were found in the midden. The general composition of JW1727 is dominated by *C. fasciatus* shells mixed with other species (*Arca* sp., *Chicoreus* sp., *Pinctada* sp.). There was little to no sedimentary matrix, although there were occasional lenses of ash, charcoal and fish bones. The *Conomurex fasciatus* shells are generally whole with low amounts of fragmentation.

Shell midden JE0087 is 200 m from the modern coastline and slightly set back behind a line of shell middens stretching along a palaeo-shoreline. The shell deposits are similar to those in JW1727 with layers of whole *C. fasciatus* shells alternating with thinner layers of fish bones and fragmented shells. There is also a larger proportion of *Chicoreus* sp. shells, which sometimes occur as distinct layers. Evidence of hearths and extensive ash layers were found, and evidence of lithics made of local limestone.

The shells analysed from JW1727 (n = 3) and JE0087 (n = 3) are typical examples and layers that are almost exclusively *C. fasciatus*-supported and are well preserved. Only one shell (JE0087-37-A-1) was taken from below a *C. fasciatus* layer where some shells were mixed into the basal sand. In JW1727 two shells were taken from layers 8 and one shell from layer 5, all date to around 4800 cal BP. Midden JE0087 is represented by two shells from layer 36 and one shell from layer 37, which both represent the older part of the midden at around 6500 cal BP.

3.3. Shell preparation and sampling for stable isotope analysis

The thick lips of adult modern shells were prepared for sclerochronological examination (Fig. 3). The shells were sectioned at 90° to the growth lines and ground with metallographic grinding paper (P800, P1250, P2500). Shells were then polished using a texmet cloth with a lubricated 3 μm diamond paste and metadi fluid, then rinsed in an ultrasound bath with ultrapure water and treated with Mutvei's solution for 20 min at c. 38 °C (Schöne et al., 2005). Growth increments were measured on a Zeiss Axioscope A1 microscope and subsequently corrected for the shell's age related decrease in growth rate by calculating the standardised growth index (SGI). For this, we first calculated the predicted growth by making use of the Bertalanffy growth function (Bertalanffy, 1938),

an exponential curve that is commonly used in estimating growth rates (Schöne, 2003; Royer et al. 2013). The equation uses $L(p)_t$ as the predicted shell length at a specific time (t), $L(p)_\infty$ as the asymptotic or ultimate length at which the growth is zero, and a growth factor K.

$$L(p)_t = L(p)_\infty * \left(1 - e^{-K*t}\right) \tag{1}$$

Using the measurements of the growth increments and nonlinear curve fitting the predicted growth were calculated. Following this, we indexed the increment measurements by dividing the length of each measured growth increment ($L_{t+1} - L_t$) at time t by the value for the predicted growth of this increment ($L(p)_{t+1} - L(p)_t$) based on Eq. (1). This produced the growth index (GI_t) for each increment.

$$GI_t = (L_{t+1} - L_t) / (L(p)_{t+1} - L(p)_t) \tag{2}$$

These indexed measurements were then standardised to create the SGI by subtracting the average growth index value (χ_{GI}) from the growth index value (GI_t) at time t and dividing the result by the standard deviation of the growth indices (σ_{GI}).

$$SGI_t = (GI_t - \chi_{GI}) / \sigma_{GI} \tag{3}$$

The shell edges of modern juvenile specimens (n = 16) were milled and the powder collected (~50 μg) for stable isotope analysis (Table 2). In addition, three juvenile specimens were used for sequential isotope analysis along the whole growth axis of the shells. The first shell, collected in February 2013 (J4-18-A length = 33 mm) was used to obtain a more detailed understanding of the change in stable isotope composition of the shell. It was sampled using a 0.9 mm drill bit from the shell-edge to the protoconch following visible growth increments on the outer shell surface with a sample width of 1 mm and a sample distance of under 1 mm. Two additional modern shells collected in May 2013 (J4-3005-A, length = 34 mm; J4-3005-C, length = 31 mm) were sampled at 2–3 mm intervals. This sampling interval was also used for all the archaeological shells, except for shells 1727-8-B-1 and 1727-8-M-2. These had thick lips at the aperture. Thickening of the lip is a common sign of adulthood (Radermacher et al., 2009) and thus we expected a different growth rate and adapted the sampling resolution. Samples were taken using a 0.4 mm drill bit at a sample distance of 0.2–0.5 mm. This procedure was carried out for the complete lip section and in a second step continued using the general sampling method to account for the changing growth rate.

Carbon and oxygen isotope analysis of the shell material ($\delta^{13}C_S$ and $\delta^{18}O_S$) was performed at the stable isotope facilities at the University of Wyoming (USA) using a Thermo Gasbench coupled to a Thermo Delta Plus XL IRMS, and at the Stable Isotope Facility of the British Geological Survey using a IsoPrime IRMS plus multiprep. Selected carbonate samples were rerun to verify comparability between laboratories. The precision in both laboratories is <0.05‰ for $\delta^{18}O$ and $\delta^{13}C$. Oxygen isotope composition of seawater ($\delta^{18}O_W$) was measured at the University of Wyoming and at the British Geological Survey using the Gasbench and IsoPrime 100 plus aquaprep, with a precision of ~0.05%. The $\delta^{18}O_W$ is reported relative to V-SMOW, $\delta^{18}O_S$ and $\delta^{13}C_S$ are reported relative to V-PDB.

$\delta^{18}O_S$ values can be used to estimate the SST at the time of shell growth by using empirically derived temperature equations. Here, we use Grossman and Ku (1986), following the adjustments for $\delta^{18}O$ of water (Dettman et al., 1999):
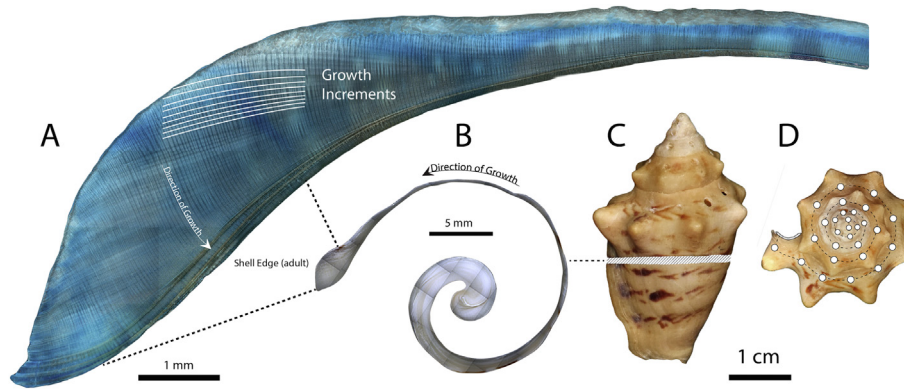
Fig. 3. Basic overview of shell anatomy. A: Mutvei stained shell section; periodic growth increments (daily) are visible in the crossed-lamellar structure of a sectioned shell (J4-2802-28), B: polished shell section; C: Complete *C. fasciatus* specimen from archaeological context (1727-5-B-1) with indication of shell section origin. Note that the shell was sectioned perpendicular to the growth lines only at the last growth increments (left side), D: Top view of *C. fasciatus* (1727-5-B-1) with sample locations for stable isotope analysis (white circles). Note the non-circular sample area at the growth edge, where carbonate was only milled.

$$\text{SST } (^{\circ}\text{C}) = 20.6 - 4.34\left(\delta^{18}\text{O}_\text{S} - \left(\delta^{18}\text{O}_\text{W} - 0.27\right)\right) \qquad (4)$$

3.4. Raman spectroscopy

Raman spectroscopy was applied to assess the mineralogical composition of modern specimens (n = 4) of *C. fasciatus* and the preservation conditions for archaeological specimens (n = 2) using a HORIBA XploRA Raman microscope. The modern specimens include three whole modern shells collected together with modern specimens specified for isotope analyses from the same point of origin (denoted here as M1-3) and a shell fragment of a modern specimen (J0004-28-C, denoted here M4) that was also used for stable isotope analysis. Archaeological specimens include shells from JW1727 (1727-8-M-2, denoted A1) and JE0087 (JE0087-37-A-1, denoted here A2), which are also part of the stable isotope analysis. All analysed fragments derive from areas that were also sampled for stable isotopes and are representative for those stable isotope values.

All fragments were ground to acquire well-mixed bulk samples. Shell M1 was measured intact to determine the mineralogical composition of the external, characteristic brown stripe, the first time that *C. fasciatus* has been characterized using Raman spectroscopy.

A large number of spectra comprising 250 and 500 spectra for each of the modern (M2-4) and archaeological (A1-2) samples, respectively, were collected from random positions on the powdered samples to ensure thorough statistical sampling. On the modern intact shell (M1), 10 spectra were collected from the characteristic brown stripe. The Raman spectra were determined as having an experimental uncertainty of ± 0.8 cm^{-1} due to instrument limitations in spectral resolution. Subsequent spectral analyses were performed using the IGOR Pro WaveMetrics software.

4. Results

4.1. Temperature, surface salinity and $\delta^{18}O_W$

Measured SSTs at Janaba Bay ranged from +26.5 °C in January 2013 (winter) to +34.9 °C in September 2013 (summer) (Fig. 2). Satellite estimates of near-shore locations have previously been shown to be inaccurate (Smit et al., 2013) and our local temperature records show occasionally higher values than the NOAA satellite

data. This is especially noticeable in the summer months, although not restricted to it. Still, the correlation between our local logger and the satellite data is very high (R^2 = 0.92). Coastal SSS values from NOAA show a little range of oscillation over the year, from 36.9 to 38.8 psu, reflecting the negligible amount of freshwater input. SST and SSS values are also within the range of what has been recorded by the NOAA in earlier years. The $\delta^{18}O_W$ values from Janaba Bay (n = 6) exhibit little variation throughout the year (Table 3), from +1.2‰ to +1.9‰ in May (Spring) and December (Winter) respectively (average value = +1.5 ± 0.3‰). In contrast, the $\delta^{18}O_W$ values from the enclosed sampling location, Khur Maadi (n = 3), have a much higher average (+2.4 ± 0.7‰) and a wider range with $\delta^{18}O_W$ values between +1.7‰ and +3.0‰ likely due to higher evaporation in the summer months.

Table 3
$\delta^{18}O_W$ isotope values and salinity measurements for collected water samples.

Location	Date	$\delta^{18}O_W$ [VSMOW]	Salinity [psu]
Janaba Bay	16. Nov 2012	+1.71	38.6
	18. Feb 2013	+1.42	37.9
	28. Feb 2013	+1.32	38.0
	30. May 2013	+1.22	37.7
	27. Sep 2013	+1.47	38.3
	11. Dec 2013	+1.94	38.4
Khur Maadi	30. May 2013	+1.67	
	27. Sep 2013	+2.52	
	11. Dec 2013	+3.02	

4.2. Growth increments

Shell growth increments at the lip of the shells range from 12.9 to 92.0 μm and display an average growth width of 38.1 ± 18 μm (Fig. 4). The predicted growth rate shows only a slight decline towards the shell edge and no pronounced drop in the overall trend is notable. The visibility of growth increments outside the lip part of the shell was extremely inconsistent despite the polishing and staining during the sample preparation.

4.3. Raman spectroscopy

Raman spectroscopy measurements on the modern shell samples M1-M4 determined the mineralogical composition of these specimens as being aragonite by comparing the key peak
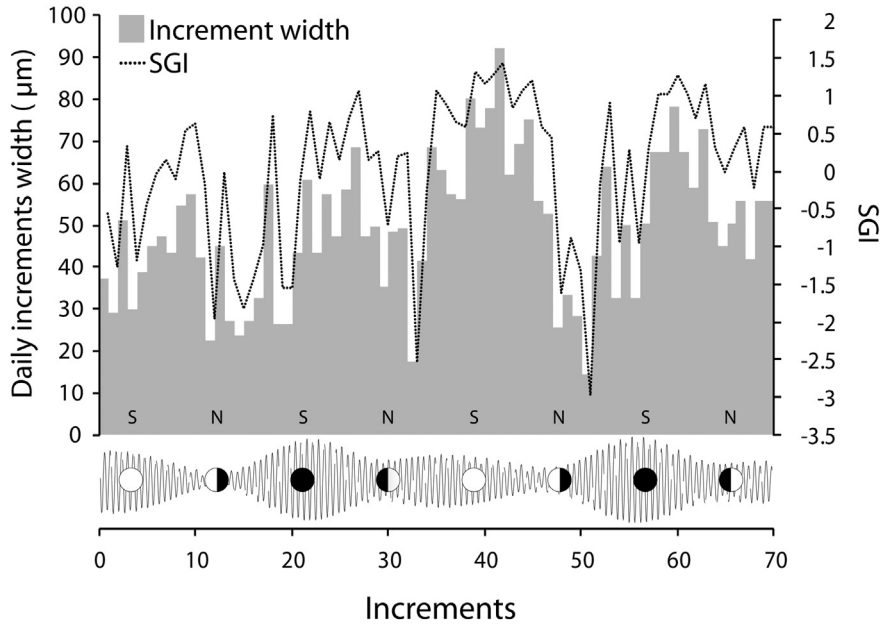
Fig. 4. Growth increment width from the shell lip of J4-2802-28 and standardized growth index (SGI). SGI removes the age-related growth trend and shows changes in increment width due to environmental and physiological forces. The frequency and the width of the increments reveal a pattern consistent with daily fluctuations closely matching the semidiurnal tidal regime over a 2 month period.

assignments identified in the figure to literature references (e.g., Urmos et al., 1991) (Fig. 5). Carotenoids were identified on the characteristic striped lines found on the external surface of intact *C. fasciatus* shells (M1), and in some of the random sampling on the powdered shell samples (M2 and M3), by comparing the peak assignments (denoted * in Fig. 5) with those discussed in Merlin (1985) and Saito and Tasumi (1983). In total, 760 spectra were obtained on the modern *C. fasciatus* shell specimens in this study to produce statistically relevant results (maximum

standard error on the averaged spectra was 8% on M1 and 5% on M2-4).

Individual spectral checking for the archaeological shell specimens showed that the entire 500 spectra-set for A1 was aragonite and that 498 spectra for A2 were aragonite with 2 spectra, containing an ad-mixture of aragonite and calcite (Fig. 6). To put this into perspective, the physical scale from which the ad-mixture occurred was within ~1 micron Raman sampling for each measurement. The low percentage occurrence (0.4%) of the ad-mixture
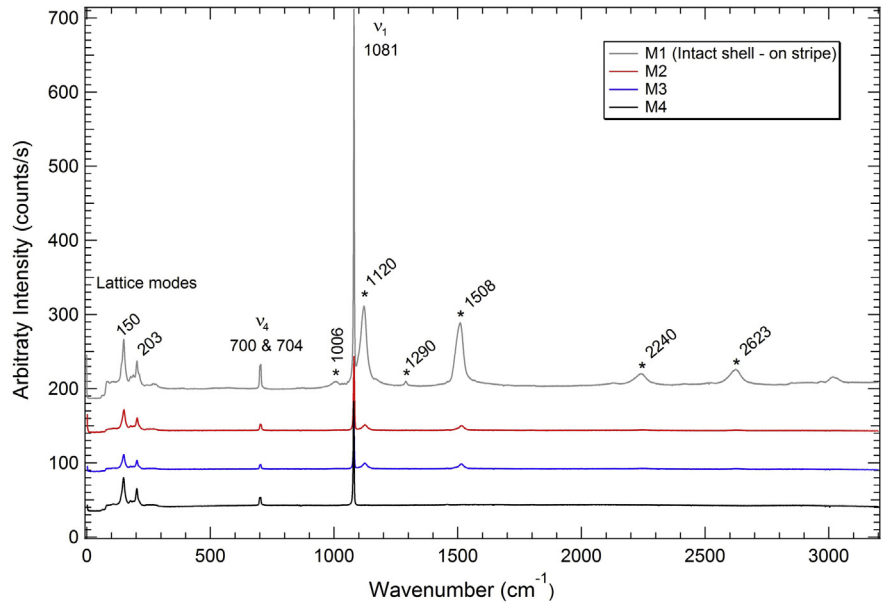

Fig. 5. Averaged Raman spectra of *C. fasciatus* obtained from (i) the characteristic stripe of an intact modern *C. fasciatus* shell (M1) comprising 10 measurements, and (ii) on the powdered modern shell specimens M2-4 comprising 250 measurements each. In total, 760 measurements were acquired on the modern shell specimens. Peaks assignments associated with aragonite are identified at 151, 204, 700, 704 and 1459 cm^{-1}. The M1-3 spectra also contain peaks (*) that are associated with carotenoids. For the analysis, a wavelength of 532 nm was used with a maximum laser power of 3.5 mW. Single spectra were acquired using the HORIBA LabSpec 6 software with 1 s of laser exposure averaged over 32 spectral repetitions.
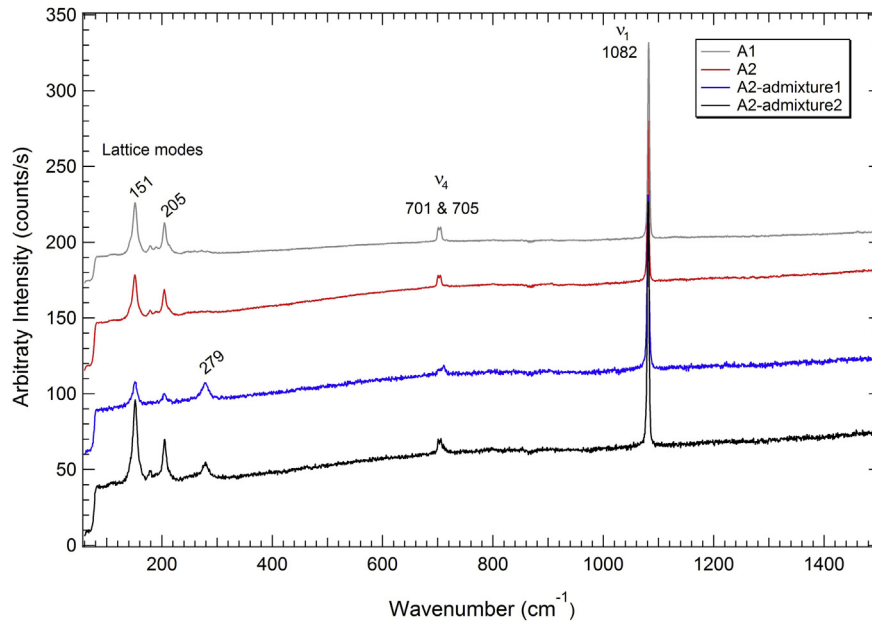
Fig. 6. Averaged Raman spectra of *C. fasciatus* obtained from (i) the powdered archaeological shell specimens from JE0087 (A1) and from JW1727 (A2), comprising 500 measurements each. The two ad-mixture spectra found in the 500 spectra sampling of A2, containing both aragonite and calcite peaks, are also shown. In total, 1000 measurements were acquired on the archaeological shell specimens. Peaks assignments associated with aragonite are identified at 151, 204, 700, 704 and 1459 cm^{-1}. A characteristic calcite peak was also determined at 279 cm^{-1} in the ad-mixture results.

justifies the large sampling. Based on this, and the 100% aragonite result found for A1, we propose that these fragment samples were well-preserved against diagenesis mechanisms that lead to an aragonite to calcite transformation.

4.4. Modern shell (shell-edge $\delta^{18}O_S$ and $\delta^{13}C_S$)

Shell-edge $\delta^{18}O_S$ values (n = 16) range from −0.5‰ to −1.7‰ ($\Delta^{18}O_S$ = 1.2‰) from February (Winter) and September (Autumn) respectively, tracking closely daily variations in NOAA's SST (R^2 = 0.84) (Table 2). Using daily SST (NOAA) and average $\delta^{18}O_W$ values the predicted shell $\delta^{18}O_S$ values (Eq. (4)) show a very good agreement with measured counterparts (R^2 = 0.88) revealing that *C. fasciatus* form the shells close or in isotopic equilibrium with the ambient water (Fig. 7). Shell-edge $\delta^{13}C_S$ values vary between +0.6‰ and +2.1‰ ($\Delta^{13}C_S$ = 1.4‰) and show a moderate positive correlation with SST (R^2 = 0.52) and a weak, inverse correlation with $\delta^{18}O_S$ (R^2 = −0.33).

4.5. Modern shell (sequential $\delta^{18}O_S$ and $\delta^{13}C_S$)

One specimen (J4-18-A) was analysed using close to continuous sampling perpendicular to the growth direction. The sequence of $\delta^{18}O_S$ values ranges from −0.3‰ to −1.6‰ and shows gradually decreasing values with increasing distance to the shell edge (Fig. 8A). The sequence of $\delta^{13}C_S$ values ranges between +1.0‰ and +1.9‰ and samples increase with increasing distance to the shell edge. As observed in shell-edge data, intra-shell $\delta^{18}O_S$ and $\delta^{13}C_S$ values are also negatively correlated (R^2 = −0.38). The two specimens collected together in May 2013 at Janaba Bay (J4-3005-A and J4-3005-C) show $\delta^{18}O_S$ values resembling a sine curve. Shell J4-3005-A ranged from −0.6‰ to −2.8‰ ($\Delta^{18}O_S$ = 2.2‰) and shell J4-3005-C from −0.5‰ to −2.5‰ ($\Delta^{18}O_S$ = 2‰). The same shells provided sequential $\delta^{13}C_S$ values ranging from +0.2‰ to +2.7‰ ($\Delta^{13}C_S$ = 2.5‰) and +0.4‰ to +1.6‰ ($\Delta^{13}C_S$ = 1.2‰) respectively (Fig. 8A). Intra-shell $\delta^{13}C_S$ and $\delta^{18}O_S$ values are negatively correlated

in J4-3005-A (R^2 = −0.33), but no correlation was found in J4-3005-C (R^2 = 0.07).

4.6. Archaeological shells ($\delta^{18}O_S$ and $\delta^{13}C_S$)

The archaeological shells dated to 4800 (JW1727) and 6500 cal BP (JE0087) show sequential $\delta^{18}O_S$ values comparable to modern specimens (Fig. 8B–D). Shells from 4800 cal BP (n = 3) exhibit $\delta^{18}O_S$ values ranging from −0.2‰ to −2.1‰ ($\Delta^{18}O_S$ = 1.9‰), whilst shells from 6500 cal BP (n = 3) show values ranging from −0.1‰ to −1.9‰ ($\Delta^{18}O_S$ = 1.8‰).

By contrast, average $\delta^{13}C_S$ values in archaeological specimens are invariably higher compared to modern counterparts (+1.3‰). Shells from archaeological contexts dated to 4800 cal BP and

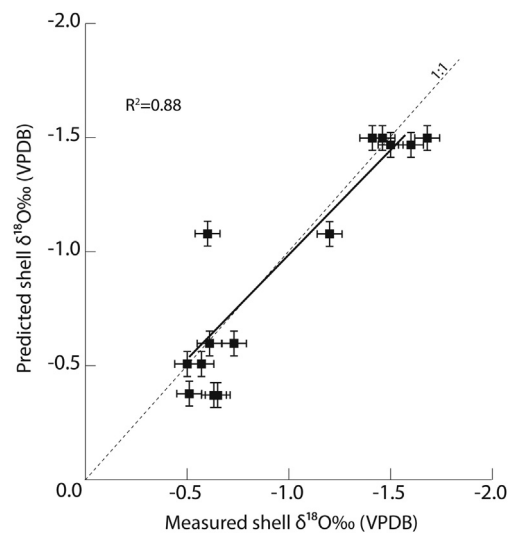**Fig. 7.** Correlation between measured average shell edge $\delta^{18}O_S$ and predicted shell edge $\delta^{18}O_W$ values using the average temperature of the month before collection.
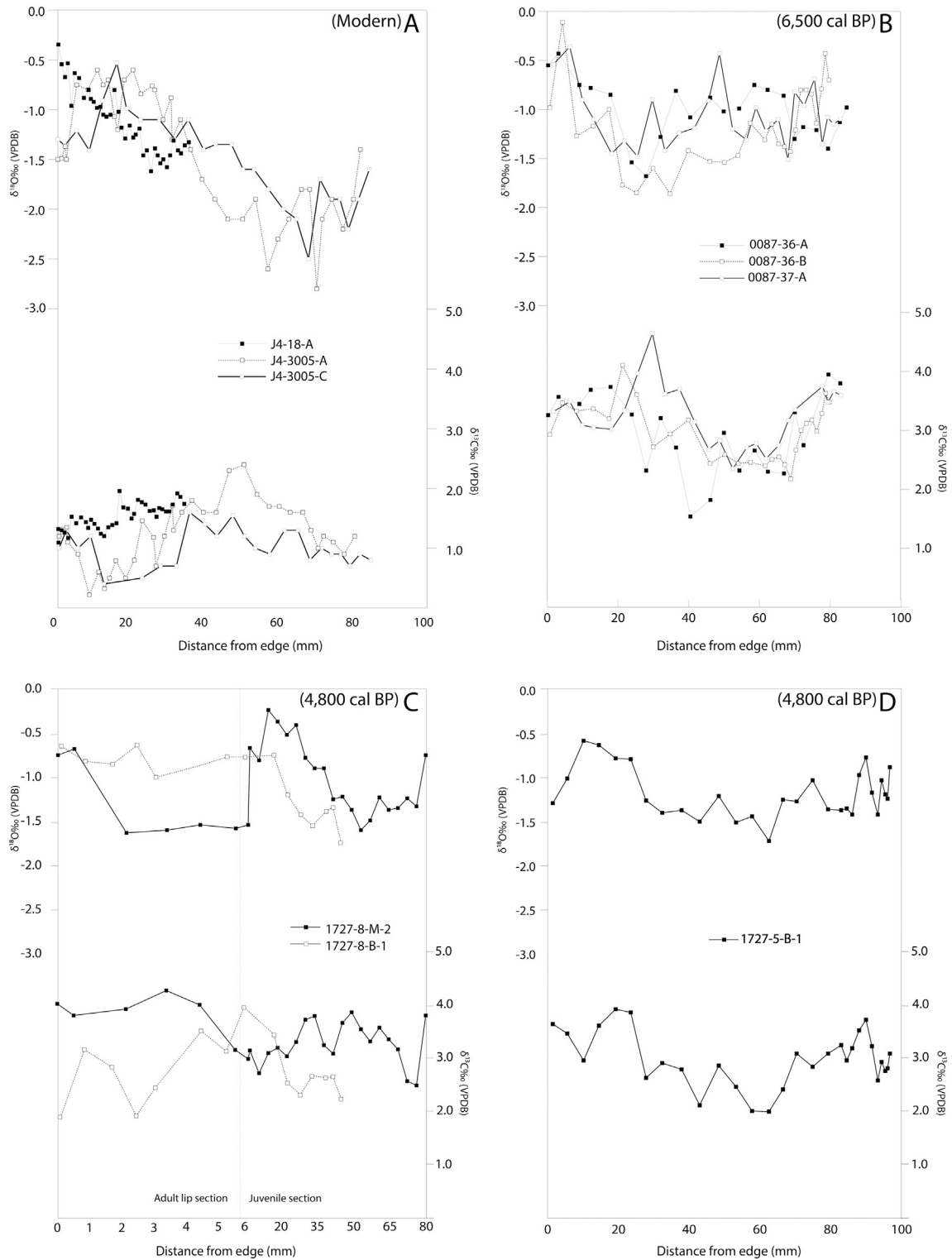
Fig. 8. A) $\delta^{18}O$ and $\delta^{13}C$ values from two shells collected on 30th May 2013 in Janaba Bay; B) $\delta^{18}O$ and $\delta^{13}C$ values from three shells dated to 6500 cal BP (JE0087); and C-D) $\delta^{18}O$ and $\delta^{13}C$ values from three shells dated to 4800 cal BP (JW1727). Notice the changing scale on the x-axis for shells in C due to the change in growth rate from lip to main body.

6500 cal BP exhibit $\delta^{13}C_S$ values ranging from +2.0‰ to +4.3‰ ($\Delta^{13}C_S$ = 2.3‰) and +1.5‰ to +4.7‰ ($\Delta^{13}C_S$ = 3.2‰), respectively. In general, no correlation between $\delta^{18}O_S$ and $\delta^{13}C_S$ was observed for archaeological shells (R^2 = 0.00 to 0.08), except for a moderately positive correlation in one shell dated to 4800 cal BP (R^2 = 0.47; 1727-5-B-1).

5. Discussion

5.1. $\delta^{18}O$ in C. fasciatus shells

The stable isotope data presented here indicate that modern *C. fasciatus* precipitates its aragonite shell close to/or in oxygen

isotope equilibrium with the ambient water in the southern Red Sea (Fig. 7). The measured $\delta^{18}O_S$ values from shell edges are also plotted on the estimated $\delta^{18}O$ values throughout the year based on the temperature data from our local dataloggers and the $\delta^{18}O_W$ values from the dates of collection (Fig. 9). The $\delta^{18}O_W$ values from between collection dates have been interpolated. The ranges of $\delta^{18}O_S$ and $\delta^{18}O_{est}$ have almost identical ranges from $-0.4‰$ to $-1.7‰$ and $-0.5‰$ to $-1.7‰$, respectively. Both ranges are smaller compared with the ranges that were recorded by the sequential $\delta^{18}O_S$ values ($-0.5‰$ to $-2.8‰$) (Fig. 8A), which is likely to be the result of the sparse seasonal collection of modern specimens in this study.

Even though precipitation is not an important factor over the study area, $\delta^{18}O_W$ can still vary significantly due to evaporation processes (Gat, 1996). As the increase of evaporation and the increase in salinity coincide with high temperatures during the summer and autumn months, the increase in $\delta^{18}O_S$ values is likely the cause of both factors, temperature and salinity. If the salinity would decrease in summer because of monsoonal rains the effects of salinity and temperature on the $\delta^{18}O_S$ composition could potentially cancel each other out in the shell record. The lack of precipitation during summer, and the fact that evaporation seems to be the main driver of salinity, both cause $\delta^{18}O_W$ to increase. This coincides with the $\delta^{18}O_W$ increase due to higher temperatures and thus makes it possible to track the seasonal changes in the shell record.

However, there are changes in $\delta^{18}O_W$ due to evaporation in the summer and autumn. This is visible when comparing $\delta^{18}O_W$ from the shell sampling area at Janaba Bay and the more enclosed Khur Maadi Bay. The lack of access to Red Sea water in Khur Maadi is likely the reason for a stronger increase in $\delta^{18}O_W$ in the warmer times of the year and the generally elevated values. For palaeotemperature analyses that use archaeological shells from the enclosed areas, this bias needs to be considered. The water samples from Janaba Bay would lead to higher palaeotemperature estimates.

Even though the water at the sampling area in Janaba Bay appears to be well mixed, it is still necessary to account for the seasonal range in $\delta^{18}O_W$ (0.7‰) when reconstructing past temperatures. A change in $\delta^{18}O_W$ of 0.7‰ can lead to a difference in estimated palaeotemperature of ~3 °C. If the annual mean $\delta^{18}O_W$ value of 1.5‰ was used to estimate the temperature using equation (4), the largest difference between measured and estimated SST would be -0.9 °C (Table 2). Using the annual mean instead of the seasonal $\delta^{18}O_W$ values will underestimate the annual range in temperature. However, due to the lack of more accurate $\delta^{18}O_W$ values for past environments the modern annual mean provides the best estimate. Combining this uncertainty of ±0.9 °C with the mean standard deviation of shell edge $\delta^{18}O$ values (±0.6 °C) (Table 2) as well as the analytical error (±0.2 °C), the uncertainty of palaeo SST estimates would be ±1.7 °C. Considering the overall

seasonal range of 8.4 °C on Farasan, this error suggests that shell carbonate $\delta^{18}O$ is a useful proxy for seasonality.

Terrestrial records of the region and marine records of the Red Sea suggest a decline in relative humidity during the Holocene connected to the southward displacement of the ITCZ and a decrease in solar insolation (Fleitmann et al., 2007), which may have affected the isotopic values of the archaeological shells. van Rampelbergh et al. (2013) compared results from speleothems, lake deposits and inter dune deposits of the southern Arabian Peninsula and found a gradual decrease in precipitation within the records at around 7000 cal BP in the lowlands. Isotope records of planktonic foraminifera *Globigerinoides ruber* from the deep-sea record of the northern and the central Red Sea show an abrupt increase in $\delta^{18}O$ values by $+0.6‰$ from 7000 to 6200 cal BP (Arz et al., 2003). The additional use of palaeotemperature records make it possible to argue for a rapid increase of salinity at the same time. Using a variety of environmental proxies, Lézine et al. (2014) found similar evidence of aridification at 6500 cal BP but with less abrupt progression.

No dramatic change in aridity or temperature has been found in our comparison of $\delta^{18}O_S$ values of specimens from 4800 (JW1727) to 6500 cal BP (JE0087). The average $\delta^{18}O_S$ values from both sites are similar and also comparable to those values recorded by modern specimens. Modern shells, however, exhibit a larger seasonal amplitude ($\Delta^{18}O_S = 2.5‰$) compared to archaeological shells ($\Delta^{18}O_S$ up to 1.9‰). This difference might imply a slightly higher seasonal contrast, with warmer summers and stronger evaporative effects happening today compared to the time of the shell mound formation. It also implies that the stable isotope composition and temperature of the marine environments from 6500 cal BP and 4800 cal BP are similar and that the environment on Farasan was already arid by 6500 cal BP.

5.2. $\delta^{13}C$ in C. fasciatus shells

Whilst $\delta^{18}O_S$ oscillation can be associated with seasonal changes in SST and $\delta^{18}O_W$, an interpretation of variations in $\delta^{13}C_S$ is much less straightforward (e.g. Andreasson et al., 1999; Gentry et al., 2008; Strauss et al., 2014). Lower $\delta^{13}C_S$ values occur during the colder months of the year and to some extent are negatively correlated with the $\delta^{18}O_S$ values (Fig. 9). Changes in $\delta^{13}C_S$ values have been linked to large salinity differences and changes in $\delta^{13}C_{DIC}$ due to freshwater input (Mook and Tan, 1991; Gillikin et al., 2006; McConnaughey and Gillikin, 2008; Owen et al., 2008). Freshwater input is minimal in the study area (36.9–38.8 psu) due to the lack of river discharge and the low levels of precipitation. The $\delta^{13}C_{DIC}$ variability could be the result of seasonal changes in the photosynthesis and circulation. Phytoplankton biomass increases from October to April (e.g. Chlorophyll-a from 0.5 mg/m^3 to 3.5 mg/m^3) as a result of the monsoon-induced surface nutrient-rich water inflow from the Indian Ocean through the Gulf of Aden (Aiki et al.,
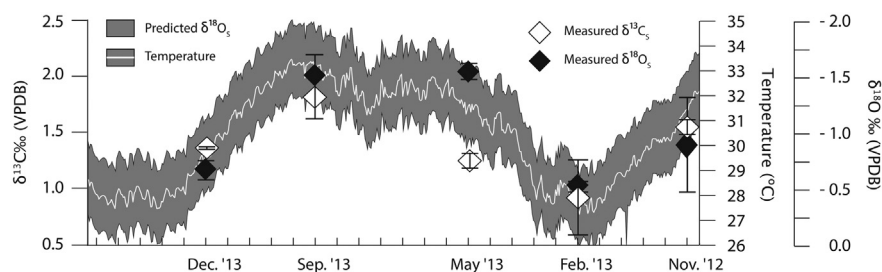

Fig. 9. Seasonal change of shell edge measurements; white diamonds: $\delta^{13}C$, black diamonds: $\delta^{18}O$. Grey area: predicted $\delta^{18}O_S$ based on NOAA temperature measurements and $\delta^{18}O_W$ values from water collected simultaneous to shell collection; white line: temperature in °C. The predicted $\delta^{18}O_S$ is illustrated with an error of one standard deviation.

2006; Raitsos et al., 2013, 2015). Additionally, during the summer monsoon nutrient water is upwelled in the Gulf of Aden (Jones and Browning, 1971) and ultimately transported into the Red Sea at an intermediate depth to eventually mix with the surface water in higher latitudes (Smeed, 1997). During photosynthesis phytoplankton preferably incorporate ^{12}C, which in turn enriches the DIC in ^{13}C (Andreasson et al., 1999). However, this mechanism would result in an increase of $\delta^{13}C_{DIC}$ in winter (and/or decrease in summer) which conflicts with the $\delta^{13}C_S$ trend observed in those seasons (Fig. 8A, Table 2). An alternative explanation is that seasonal $\delta^{13}C_S$ variability, to some extent, reflects changes in food availability between warmer and colder months. C. fasciatus predominantly feeds on interstitial microflora and detritus (Taylor and Reid, 1984) and although DIC may have a prevailing influence on $\delta^{13}C_S$ values of C. fasciatus, increased feeding on algae during colder months may result in a larger contribution of metabolic carbon relative to shell carbon (e.g. Chauvaud et al., 2011). This mechanism could be responsible for lower $\delta^{13}C_S$ values in colder months. However to what degree the metabolic carbon contribute to $\delta^{13}C_S$ values in C. fasciatus is difficult to ascertain. There is no indication of an increase in growth rate that would correspond with an increase in food availability.

The $\delta^{13}C_S$ values notably differ between archaeological and modern samples (Fig. 8A—D). Despite modern and archaeological shells displaying similar seasonal $\delta^{13}C_S$ variability ($\Delta^{13}C_S = 2.5‰$), the archaeological specimens have higher $\delta^{13}C_S$ values (~2‰) compared to modern counterparts. High $\delta^{13}C_S$ in middle-late Holocene shells in the southern Red Sea is difficult to explain. A general $\delta^{13}C$ increase of 1—1.5‰ is expected for carbonate records that predate the industrial revolution and the accompanying increase of ^{12}C in the atmosphere due to the burning of fossil fuels (Friedli et al., 1986; Sonnerup et al., 1999; Surge et al., 2003). In marine records this effect is more moderate due to mixing of surface and deeper (older) waters (Cage and Austin, 2010), but between 1970 and 1990 the mean global surface ocean $\delta^{13}C$ values still decreased by $0.16 \pm 0.02‰$ (Quay et al., 2003). Consequently, the oceanic Suess effect could largely explain almost all of the ^{13}C-enrichment of the shell.

An alternative, or additional explanation, could be an overall increase in $\delta^{13}C_{DIC}$ in the southern Red Sea. ^{13}C-enrichment in seawater DIC is often interpreted as the product of an increased nutrient supply and increased rate of photosynthetic activity in surface water (McConnaughey, 2003). Today, summer monsoon is responsible for lateral advection of nutrient-rich water from the northern Arabian Sea into the Red Sea. The injection of upwelled water from the Gulf of Aden controls the vertical nutrient recycling and increase primary productivity in this region (Bouilloux et al., 2013). Even though the ITCZ had moved too far south to sustain a humid environment in Arabia (Fleitmann et al., 2007; van Rampelbergh et al., 2013), the injection of nutrient rich water due to monsoonal activity from the Arabian Sea into the southern Red will still have contributed to the upwelling effect in the Arabian Sea and consequently contributed to the injection of nutrients into the southern Red Sea (Raitsos et al., 2013, 2015).

Although further studies are required to fully understand the substantial ^{13}C-enrichment in middle-late Holocene shells compared to modern counterparts, it is worth noting that the vast amounts of shell material accumulated in the Farasan shell middens most likely indicate a highly productive marine environment (Meredith-Williams et al., 2014b). It remains to be assessed if such regional economic practices, uniquely represented by thousands of shell mounds along the coastline, ultimately reflect periods of heightened marine productivity, which today is modulated by monsoon atmospheric circulation.

5.3. Implications for the use of C. fasciatus as seasonal environmental archives

Analyses of C. fasciatus have shown several factors that need to be considered when using the mollusc as an environmental proxy. Chiefly, the unclear and changing growth patterns between adult and juvenile parts of the shell are of concern. The almost continuous sequence of $\delta^{18}O_S$ values in the juvenile modern shell J4-18-A (Fig. 8A) indicates a gradual change from higher temperatures to lower temperatures towards the shell edge. The slow isotopic change over a 35 mm long distance demonstrates a very rapid shell production for juvenile specimens. This is similarly evident in longer sequences over 80 mm (J4-3005-A and J4-3005-C). However, not all specimens are juvenile, and the different growth patterns in adult areas of the shell need to be part of the analysis to create longer sequences than the one-year sequence that was recorded in the juvenile shells (J4-3005-A and J4-3005-C).

Previously, a similar change in the growth pattern has been reported for Strombus gigas, where after about two years adult specimens develop a thick lip at the aperture by depositing only a few mm of shell carbonate each month (Radermacher et al., 2009). To analyse the adult growth patterns in our assemblage, the lip part of adult modern shells was chosen and their growth increments measured. The frequency and the width of the increments revealed a repeating pattern with a period of 14—16 increments (Fig. 4). This pattern was compared to the periodicity of the tidal regime (0.6 m) at Farasan using WXtide32 (available at www.wxtide32.com). The tidal fluctuations around the study occur in fortnightly cycles almost identical to the 14—16 increments period of growth rate fluctuation. This similarity has been observed in previous studies of subtidal molluscs (Schöne, 2003; Schöne and Giere, 2005; Schöne et al., 2007), where in all cases the shell growth rate decreased during neap tides. Considering the similar periodicity of small growth increments, it is plausible that this connection can also be proposed for C. fasciatus shells. Despite the smaller influence that neap tides have on subtidal gastropods, there likely is an endogenous component that controls the rhythmicity of shell growth even without a dramatic exterior impetus (Brown et al., 1955a,b). Additionally, the decreased water-exchange during neap tides could have an effect on subtidal organisms. Following this, the growth increments are daily and follow fortnightly cycles and show an average growth of 38.1 ± 18 μm. Using this number as a rough estimate, we can assume a growth rate of ~13 mm/year. This estimate is only applicable to the shell edge of adult specimens. The growth rate in juvenile parts of the shell remains unclear due to the inconsistent visibility of growth increments. However, sequential $\delta^{18}O_S$ values from J4-3005-A and J4-3005-C are likely to show a one-year record over ~90 mm, which gives an estimate of growth.

The contrast between a fast and a slow growth rate in each shell introduces some problems. From the analysed growth increments it is not clear, when exactly this change occurs as the visibility vastly decreases before any change in growth was measurable. Also, it is not clear if the change in growth patterns is gradual over several months, or happens over a period of a few days or weeks. To fully connect the two parts of the shell in a sequence of values, the sampling resolution needs to be high enough to rule out the possibility that some periods of growth have been missed. In the analysed shells with changing sampling resolutions, the transition was recorded well (Fig. 8C) with similar $\delta^{18}O_S$ values of the four measurements (JW1727-8-B-1: −0.84‰, −0.75‰, −0.75‰, −0.73‰; JW1727-8-M-2: −1.60‰, −1.54‰, −1.58‰, −1.54‰) across the transition (dotted line) over a length of ~10 mm. Our results demonstrate that the sampling strategy

allows for the recovery of environmental information spanning from fortnightly to monthly time-intervals. This does not rule out other causes of growth hiatuses such as storm events, pathological problems, or attacks by predators.

6. Conclusions

1) Modern *C. fasciatus* from the southern Red Sea precipitate their shells close to equilibrium with the oxygen isotope composition of the surrounding seawater at a given temperature according to the palaeotemperature equation of Grossman and Ku (1986).
2) Over an annual cycle $\delta^{18}O_S$ from *C. fasciatus* records the full range of SST without apparent growth hiatuses. *C. fasciatus* reach maturity (with continual growth) in about a year.
3) Sequential $\delta^{18}O_S$ of daily growth increments within shell and lip sections of adult *C. fasciatus* show that the animal grows very fast (80–90 mm) in the first year. Then, there is a considerable decrease in growth rate on reaching adulthood when the lip thickens (~13 mm). Both growth rates are sufficiently fast to avoid time averaging and the sampling resolution is high enough for seasonal-palaeoclimate studies.
4) $\delta^{13}C_S$ values of *C. fasciatus* are likely a function of food availability and changing $\delta^{13}C_{DIC}$ of seawater in this region which could be used as a seasonal proxy for primary productivity.

Acknowledgements

Appendix A. Supplementary data

Supplementary data related to this article can be found at http://dx.doi.org/10.1016/j.quaint.2015.08.051.

References

Adamson, D.A., Gasse, F., Street, F.A., Williams, M.A.J., 1980. Late Quaternary history of the Nile. Nature 288, 50–55.

Aiki, H., Takahashi, K., Yamagata, T., 2006. The Red Sea outflow regulated by the Indian monsoon. Continental Shelf Research 26 (12), 1448–1468.

Alsharekh, A., Bailey, G., 2014. Coastal Prehistory in Southwest Arabia and the Farasan Islands: 2004–2009 Field Investigations. Saudi Commission for Tourism and Antiquities, Riyadh.

Andrus, C.F.T., 2011. Shell midden sclerochronology. Quaternary Science Reviews 30, 2892–2905.

Andreasson, F.P., Schmitz, B., Jönsson, E., 1999. Surface-water seasonality from stable isotope profiles of *Littorina littorea* shells: implications for paleoenvironmental reconstructions of coastal areas. Palaios 273–281.

Arrighetti, F., Teso, V., Brey, T., Mackensen, A., Penchaszadeh, P.E., 2012. Age and growth of *Olivancillaria deshayesiana* (Gastropoda: Olividae) in the southwestern Atlantic Ocean. Malacologia 55 (1), 163–170.

Arz, H.W., Lamy, F., Pätzold, J., Muller, J.P., Prins, M., 2003. Mediterranean moisture source for an Early Holocene humid period in the northern Red Sea. Science 300, 118–121.

Bailey, G.N., Flemming, N.C., King, G.C.P., Lambeck, K., Momber, G., Moran, L.J., Al-Sharekh, A., Vita-Finzi, C., 2007. Coastlines, submerged landscapes, and Human Evolution: the Red Sea Basin and the Farasan Islands. Journal of Island and Coastal Archaeology 2, 127–160.

Bailey, G.N., Meredith-Williams, M.G., Alsharekh, A.M., 2013. Shell Mounds of the Farasan Islands, Saudi Arabia. In: Bailey, G.N., Hardy, K., Camara, A. (Eds.), Shell Energy, pp. 241–254.

Bantan, R.A., 1999. Geology and Sedimentary Environments of Farasan Bank (Saudi Arabia) Southern Red Sea: a Combined Remote Sensing and Field Study (unpublished PhD dissertation). University of London, United Kingdom.

Bar-Matthews, M., Ayalon, A., Kaufman, A., Wasserburg, G.J., 1999. The Eastern Mediterranean paleoclimate as a reflection of regional events: Soreq cave, Israel. Earth and Planetary Science Letters 166, 85–95.

Bertalanffy, L. v, 1938. A quantitative theory of organic growth. Human Biology 10, 181–213.

Biton, E., Gildor, H., Trommer, G., Siccha, M., Kucera, M., Van Der Meer, M.T.J., Schouten, S., 2010. Sensitivity of Red Sea circulation to monsoonal variability during the Holocene: an integrated data and modelling study. Paleoceanography 25 (4), 4209.

Bouilloux, A., Valet, J.P., Bassinot, F., Joron, J.L., Dewilde, F., Blanc-Valleron, M.M., Moreno, E., 2013. Influence of seawater exchanges across the Bab-el-Mandeb Strait on sedimentation in the Southern Red Sea during the last 60 ka. Paleoceanography 28 (4), 675–687.

Bray, H.E., Stokes, S., 2004. Temporal patterns of arid-humid transitions in the south-eastern Arabian Peninsula based on optical dating. Geomorphology 59 (1), 271–280.

Brown Jr., F.A., Webb, H.M., Bennett, M.F., 1955a. Proof for an endogenous component in persistent solar and lunar rhythmicity in organisms. Proceedings of the National Academy of Sciences of the United States of America 41 (2), 93.

Brown, F.A., Webb, H.M., Bennett, M.F., Sandeen, M.I., 1955b. Evidence for an exogenous contribution to persistent diurnal and lunar rhythmicity under so-called constant conditions. The Biological Bulletin 109 (2), 238–254.

Bruckner, A., Rowlands, G.P., Riegl, B., Purkis, S., Williams, A., Renaud, P., 2011. Atlas of Saudi Arabian Red Sea Marine Habitats. Panoramic Press.

Cage, A.G., Austin, W.E., 2010. Marine climate variability during the last millennium: the Loch Sunart record, Scotland, UK. Quaternary Science Reviews 29, 1633–1647.

van Campo, E., Duplessy, J.-C., Rossignol-Strick, M., 1982. Climatic conditions deduced from a 150 kyr oxygen isotope-pollen record from the Arabian Sea. Nature 296, 56–59.

Chauvaud, L., Thébault, J., Clavier, J., Lorrain, A., Strand, Ø., 2011. What's hiding behind ontogenetic $\delta^{13}C$ variations in mollusk shells? New insights from the great scallop (*Pecten maximus*). Estuaries and Coasts 34 (2), 211–220.

Colonese, A.C., Troelstra, S., Ziveri, P., Martini, F., Lo Vetro, D., Tommasini, S., 2009. Mesolithic shellfish exploitation in SW Italy: seasonal evidence from the oxygen isotopic composition of *Osilinus turbinatus* shells. Journal of Archaeological Science 36 (9), 1935–1944.

Cornu, S., Pätzold, J., Bard, E., Meco, J., Cuerda-Barcelo, J., 1993. Paleotemperature of the last interglacial period based on $\delta^{18}O$ of *Strombus bubonius* from the western Mediterranean Sea. Palaeogeography, Palaeoclimatology, Palaeoecology 103 (1), 1–20.

Dettman, D.L., Reische, A.K., Lohmann, K.C., 1999. Controls on the stable isotope composition of seasonal growth bands in aragonitic freshwater bivalves (Unionidae). Geochimica et Cosmochimica Acta 63, 1049–1057.

Durrani, N., 2005. The Tihamah Coastal Plain of South-west Arabia in its Regional Context, c. 6000 BC–AD 600. In: British Archaeological Reports 1456. Archaeopress.

Finstad, K.M., Ingram, B.L., Schweikhardt, P., Lightfoot, K.G., Luby, E.M., Coles, G.R., 2013. New insights about the construction and use of shell mounds from the geochemical analysis of mollusks: an example from the greater San Francisco Bay. Journal of Archaeological Science 40, 2648–2658.

Fleitmann, D., Burns, S.J., Mangini, A., Mudelsee, M., Kramers, J., Villa, I., Neff, U., Al-Subbary, A., Buettner, A., Hippler, D., Matter, A., 2007. Holocene ITCZ and Indian monsoon dynamics recorded in stalagmites from Oman and Yemen (Socotra). Quaternary Science Reviews 26, 170–188.

Friedli, H., Lötscher, H., Oeschger, H., Siegenthaler, U., Stauffer, B., 1986. Ice core record of the $^{13}C/^{12}C$ ratio of atmospheric CO_2 in the past two centuries. Nature 324, 237–238.

Gasse, F., 2000. Hydrological changes in the African tropics since the Last Glacial Maximum. Quaternary Science Reviews 19, 189–211.

Gat, J.R., 1996. Oxygen and hydrogen isotopes in the hydrologic cycle. Annual Review of Earth and Planetary Sciences 24 (1), 225–262.

Geary, D.H., Brieske, T.A., Bemis, B.E., 1992. The influence and interaction of temperature, salinity, and upwelling on the stable isotopic profiles of strombid gastropod shells. Palaios 77–85.

Gentry, D.K., Sosdian, S., Grossman, E.L., Rosenthal, Y., Hicks, D., Lear, C.H., 2008. Stable isotope and Sr/Ca profiles from the marine gastropod *Conus ermineus*: testing a multiproxy approach for inferring paleotemperature and paleosalinity. Palaios 23, 195–209.

Gillikin, D.P., Lorrain, A., Bouillon, S., Willenz, P., Dehairs, F., 2006. Stable carbon isotopic composition of *Mytilus edulis* shells: relation to metabolism, salinity, $\delta^{13}C_{DIC}$ and phytoplankton. Organic Geochemistry 37 (10), 1371–1382.

Gillikin, D.P., Lorrain, A., Meng, L., Dehairs, F., 2007. A large metabolic carbon contribution to the $\delta^{13}C$ record in marine aragonitic bivalve shells. Geochimica et Cosmochimica Acta 71 (12), 2936—2946.

Grossman, E.L., Ku, T.-L., 1986. Oxygen and carbon isotope fractionation in biogenic aragonite: temperature effects. Chemical Geology 59, 59—74.

Hoelzmann, P., Jolly, D., Harrison, S.P., Laarif, F., Bonnefille, R., Pachur, H.J., 1998. Mid-Holocene land-surface conditions in northern Africa and the Arabian Peninsula: a data set for the analysis of biogeophysical feedbacks in the climate system. Global Biogeochemical Cycles 12, 35—51.

Jones, E.N., Browning, D.G., 1971. Cold water layer in the southern Red Sea. Limnology and Oceanography 16 (3), 503—509.

Leng, M.J., Lewis, J.P., 2014. Oxygen isotopes in Molluscan shell: applications in environmental archaeology. Environmental Archaeology. http://dx.doi.org/10.1179/1749631414Y.0000000048.

Lézine, A.M., Bassinot, F., Peterschmitt, J.Y., 2014. Orbitally-induced changes of the Atlantic and Indian monsoons over the past 20,000 years: new insights based on the comparison of continental and marine records. Bulletin de la Societe Geologique de France 185 (1), 3—12.

Mannino, M.A., Spiro, B.F., Thomas, K.D., 2003. Sampling shells for seasonality: oxygen isotope analysis on shell carbonates of the intertidal gastropod *Monodonta lineata* (da Costa) from populations across its modern range and from a Mesolithic site in southern Britain. Journal of Archaeological Science 30 (6), 667—679.

McConnaughey, T.A., 2003. Sub-equilibrium oxygen-18 and carbon-13 levels in biological carbonates: carbonate and kinetic models. Coral Reefs 22 (4), 316—327.

McConnaughey, T.A., Gillikin, D.P., 2008. Carbon isotopes in mollusk shell carbonates. Geo-Marine Letters 28, 287—299.

Meredith-Williams, M.G., Hausmann, N., Bailey, G.N., King, G.C.P., Alsharekh, A., Al Ghamdi, S., Inglis, R.H., 2014a. Mapping, modelling and predicting prehistoric coastal archaeology in the southern Red Sea using new applications of digital-imaging techniques. World Archaeology 46.1, 10—24.

Meredith-Williams, M., Hausmann, N., Inglis, R., Bailey, G., 2014b. 4200 New shell Mound sites in the Southern Red Sea. In: Fernandes, R., Meadows, J. (Eds.), 'Human Exploitation of Aquatic Landscapes' Special Issue. http://dx.doi.org/10.11141/ia.37.2. Internet Archaeology.

Merlin, J.C., 1985. Resonance Raman spectroscopy of carotenoids and carotenoid containing systems. Pure and Applied Chemistry 57 (5), 785—792.

Mook, W.G., Tan, F.C., 1991. Stable carbon isotopes in rivers and estuaries. Biogeochemistry of Major World Rivers 42, 245—264.

Owen, E.F., Wanamaker Jr., A.D., Feindel, S.C., Schöne, B.R., Rawson, P.D., 2008. Stable carbon and oxygen isotope fractionation in bivalve *Placopecten magellanicus* larval aragonite. Geochimica et Cosmochimica Acta 72 (19), 4687—4698.

Pachur, H.J., Kröpelin, S., 1987. Wadi Howar: Paleoclimatic evidence from an extinct river system in the southeastern Sahara. Science 237, 298—300.

Quay, P., Sonnerup, R., Westby, T., Stutsman, J., McNichol, A., 2003. Changes in the $^{13}C/^{12}C$ of dissolved inorganic carbon in the ocean as a tracer of anthropogenic CO_2 uptake. Global Biogeochemical Cycles 17 (1), 4—1.

Radermacher, P., Schöne, B.R., Gischler, E., Oschmann, W., Thébault, J., Fiebig, J., 2009. Sclerochronology — a highly versatile tool for mariculture and reconstruction of life history traits of the queen conch, *Strombus gigas* (Gastropoda). Aquatic Living Resources 22, 307—318.

Raitsos, D.E., Pradhan, Y., Brewin, R.J., Stenchikov, G., Hoteit, I., 2013. Remote sensing the phytoplankton seasonal succession of the Red Sea. PloS One 8 (6), e64909.

Raitsos, D.E., Yi, X., Platt, T., Racault, M.F., Brewin, R.J., Pradhan, Y., Papadopoulos, V.P., Sathyendranath, S., Hoteit, I., 2015. Monsoon oscillations regulate fertility of the Red Sea. Geophysical Research Letters 42 (3), 855—862.

van Rampelbergh, M., Fleitmann, D., Verheyden, S., Cheng, H., Edwards, L., de Geest, P., de Vleeschouwer, D., Burns, S.J., Matter, A., Claeys, P., Keppens, E., 2013. Mid-to late Holocene Indian Ocean Monsoon variability recorded in four speleothems from Socotra Island, Yemen. Quaternary Science Reviews 65, 129—142.

Rossignol-Strick, M., 1983. African monsoons, an immediate climate response to orbital insolation. Nature 304, 46—49.

Rossignol-Strick, M., 1985. Mediterranean Quaternary sapropels, an immediate response of the African Monsoon to variation of insolation. Palaeogeography, Palaeoclimatology, Palaeoecology 49, 237—263.

Royer, C., Thébault, J., Chauvaud, L., Olivier, F., 2013. Structural analysis and paleoenvironmental potential of dog cockle shells (*Glycymeris glycymeris*) in Brittany, northwest France. Palaeogeography, Palaeoclimatology, Palaeoecology 373, 123—132.

Saito, S., Tasumi, M., 1983. Normal-coordinate analysis of β-carotene isomers and assignments of the Raman and Infrared bands. Journal of Raman Spectroscopy 14, 310—321.

Schöne, B.R., 2003. A 'clam-ring' master-chronology constructed from a short-lived bivalve mollusc from the northern Gulf of California, USA. The Holocene 13, 39—49.

Schöne, B.R., 2008. The curse of physiology—challenges and opportunities in the interpretation of geochemical data from mollusk shells. Geo-Marine Letters 28 (5—6), 269—285.

Schöne, B.R., Giere, O., 2005. Growth increments and stable isotope variation in shells of the deep-sea hydrothermal vent bivalve mollusk Bathymodiolus brevior from the North Fiji Basin, Pacific Ocean. Deep Sea Research Part I: Oceanographic Research Papers 52 (10), 1896—1910.

Schöne, B.R., Dunca, E., Fiebig, J., Pfeiffer, M., 2005. Mutvei's solution: an ideal agent for resolving microgrowth structures of biogenic carbonates. Palaeogeography, Palaeoclimatology, Palaeoecology 228 (1), 149—166.

Schöne, B.R., Rodland, D.L., Wehrmann, A., Heidel, B., Oschmann, W., Zhang, Z., Fiebig, J., Beck, L., 2007. Combined sclerochronologic and oxygen isotope analysis of gastropod shells (Gibbula cineraria, North Sea): life-history traits and utility as a high-resolution environmental archive for kelp forests. Marine Biology 150 (6), 1237—1252.

Schweikhardt, P., Ingram, B.L., Lightfoot, K., Luby, E., 2011. Geochemical methods for inferring seasonal occupation of an estuarine shellmound: a case study from San Francisco Bay. Journal of Archaeological Science 38 (9), 2301—2312.

Sharabati, D., 1984. Red sea shells, Routledge Kegan & Paul.

Siddall, M., Smeed, D.A., Hemleben, C., Rohling, E.J., Schmelzer, I., Peltier, W., 2004. Understanding the Red Sea response to sea level. Earth and Planetary Science Letters 225, 421—434.

Sirocko, F., Sarthein, M., Erlenkeuser, H., Lange, H., Arnold, M., Duplessy, J.-C., 1993. Century-scale events in monsoonal climate over the past 24,000 years. Nature 364, 322—324.

Smeed, D., 1997. Seasonal variation of the flow in the strait of Bah al Mandab. Oceanolica Acta 20 (6), 773—781.

Smit, A.J., Roberts, M., Anderson, R.J., Dufois, F., Dudley, S.F., Bornman, T.G., Olbers, J., Bolton, J.J., 2013. A coastal seawater temperature dataset for biogeographical studies: large biases between in situ and remotely-sensed data sets around the coast of South Africa. Plos One. http://dx.doi.org/10.1371/journal.pone.0081944.

Sonnerup, R.E., Quay, P.D., McNichol, A.P., Bullister, J.L., Westby, T.A., Anderson, H.L., 1999. Reconstructing the oceanic ^{13}C Suess effect. Global Biogeochemical Cycles 13 (4), 857—872.

Strauss, J., Oleinik, A., Swart, P., 2014. Stable isotope profiles from subtropical marine gastropods of the family Fasciolariidae: growth histories and relationships to local environmental conditions. Marine Biology 1—10.

Surge, D.M., Lohmann, K.C., Goodfriend, G.A., 2003. Reconstructing estuarine conditions: oyster shells as recorders of environmental change, Southwest Florida. Estuarine, Coastal and Shelf Science 57 (5), 737—756.

Taylor, J.D., Reid, D.G., 1984. The abundance and trophic classification of molluscs upon coral reefs in the Sudanese Red Sea. Journal of Natural History 18 (2), 175—209.

Thomas, K.D., 2015. Molluscs emergent, Part I: themes and trends in the scientific investigation of mollusc shells as resources for archaeological research. Journal of Archaeological Science 56, 133—140.

Trommer, G., Siccha, M., Rohling, E.J., Grant, K., van der Meer, M.T.J., Schouten, S., Hemleben, C., Kucera, M., 2010. Millennial-scale variability in Red Sea circulation in response to Holocene insolation forcing. Paleoceanography 25 (26).

Urmos, J., Sharma, S., Mackenzie, F., 1991. Characterization of some biogenic carbonates with Raman spectroscopy. American Mineralogist 76, 641—646.

Walls, J.G., 1980. Conchs, Tibias, and Harps. T.F.H. Publications, Hong Kong.

Wefer, G., Killingley, J.S., 1980. Growth histories of strombid snails from Bermuda recorded in their O-18 and C-13 profiles. Marine Biology 60 (2—3), 129—135.

Zarins, J., Murad, A., al-Yish, K., 1981. Comprehensive archaeological survey program: the second preliminary report on the Southwestern Province. Atlal 5, 9—42.